Journal of Applied Physics ARTICLE scitation.org/journal/jap

The role of momentum conservation on the tunneling between a two-dimensional electron gas and self-assembled quantum dots

Cite as: J. Appl. Phys. **132**, 064401 (2022); doi: 10.1063/5.0098561
Submitted: 10 May 2022 · Accepted: 15 July 2022 ·
Published Online: 9 August 2022

Daming Zhou,[1,2,a)] Jens Kerski,[2] Andreas Beckel,[2] Martin Geller,[2] Axel Lorke,[2] Arne Ludwig,[3] Andreas D. Wieck,[3] Xiaoshuang Chen,[1] and Wei Lu[1]

AFFILIATIONS

[1]Chongqing Institute of Green and Intelligent Technology, Chinese Academy of Sciences, 400714 Chongqing, China and National Laboratory for Infrared Physics, Shanghai Institute of Technical Physics, Chinese Academy of Sciences, Shanghai 200083, China
[2]Faculty of Physics and CENIDE, University of Duisburg-Essen, Lotharstraße 1, 47057 Duisburg, Germany
[3]Lehrstuhl für Angewandte Festkörperphysik, Ruhr-Universität Bochum, Universitätstraße 150, 44780 Bochum, Germany

[a)]**Author to whom correspondence should be addressed:** dmzhou@cigit.ac.cn

ABSTRACT

The electron tunneling rates between a two-dimensional electron gas (2DEG) and self-assembled InAs quantum dots are studied by applying a magnetic field perpendicular to the tunneling direction. For both the ground and the first excited states, the tunneling rate can be modified by a magnetic field. The field dependence of both the *s* and *p* state tunneling rates can be explained with a model, based on momentum matching between the Fermi surface of the 2DEG and the wave function of the quantum dots in momentum space. The results, together with the comparison between charging and discharging rates, provide insight into the filling sequence of the p-state electrons.

I. INTRODUCTION

Self-assembled quantum dots (QDs) have continuously attracted scientific attention during the past decades, due to their possible application for non-volatile memory[1–6] and quantum technology devices.[7,8] While modern devices are scaled down to nanometers, quantum effects emerge naturally. Consequently, the fundamental physical mechanisms of quantum dot devices are necessarily studied. For memory devices, the coupling between the dot and a two-dimensional electron gas (2DEG) in field-effect transistor structures is of particular interest.

Previously, using capacitance–voltage ($C-V$) spectroscopy and far-infrared spectroscopy, the many-particle ground states of the dots have been investigated in detail.[9–11] An equivalent capacitance–resistance circuit can be derived from the frequency-dependent measurements.[12] Furthermore, with an external magnetic field B_z being applied in the tunneling direction, not only the magnitude of the wave function but also the sign of the phase factor can be gauged. This results from the fact that a magnetic field in the growth direction B_z imposes an angular momentum direction on the emitter states and thus influences the tunneling into QD states if their angular momentum has the same or opposite sign as the emitter states.[13] Furthermore, the injection of single electrons from the 2DEG into the quantum dots can be demonstrated either for the equilibrium or non-equilibrium tunneling dynamics (i.e., tunneling into ground or exciting states, respectively).[14,15] In the experiment, a 2DEG is not only used as a charge reservoir but also as a detector to monitor the charging and discharging processes of the quantum dots.[16,17] By applying a voltage pulse to the gate of the field-effect transistor, the QDs can be charged (discharged), so that the channel conductance decreases (increases) exponentially, accompanying the transfer of charge from the 2DEG to the quantum dots (or vice versa). By evaluating the time dependence of the conductance, one can obtain the electron tunneling rate, which reflects the wave-function overlap between the dots and the free electrons in the 2DEG.

II. EXPERIMENT

The investigated samples are GaAs/$Al_{0.34}Ga_{0.66}$As heterostructure transistors, grown by molecular beam epitaxy, with embedded

InAs quantum dots. On a semi-insulating GaAs(001) substrate, a 200 nm thick GaAs buffer is grown, followed by a 40-period superlattice, consisting of an alternating sequence of 2 nm thick AlAs and 2 nm thick GaAs. On top of this structure, an inverted high-electron-mobility transistor was deposited consisting of 300 nm $Al_{0.34}Ga_{0.66}As$, a Si delta doping layer, followed by a 16 nm $Al_{0.34}Ga_{0.66}As$ spacer layer and a 15 nm GaAs quantum well. Subsequently, 10 nm $Al_{0.34}Ga_{0.66}As$ and 5 nm GaAs were grown as a tunneling barrier. For the QDs, 1.9 ML of InAs was deposited at 525 °C and covered with 30 nm GaAs. Finally, a 116 nm AlAs/GaAs superlattice blocking layer and a 5 nm GaAs cap layer complete the heterostructure. The chips in the work were from the same wafer as the experiment in Ref. 15. The quantum dots had a typical height of a few nanometers and diameter of a few tens of nanometers, with an area density of $8.3 \times 10^9\,\mathrm{cm}^{-2}$, which was determined by atomic force microscopic studies of similarly grown dots on the sample surface.[15,18] The wafer was cleaved into $4 \times 4\,\mathrm{mm}^2$ pieces, and by optical lithography, lift-off and wet chemical etching, field-effect transistors were patterned. A layer of Ni/AuGe/Au was evaporated and annealed at 430 °C for Ohmic source and drain contacts. Afterwards, the gate electrode was fabricated, using Ti and Au evaporation. The device structure and schematic cross section of the layer sequence are shown in Figs. 1(a) and 1(b). All measurements were performed at 4.2 K in a liquid-He cryostat equipped with a superconducting solenoid. Magnetic fields up to 12 T could be applied.

A. Many-particle energy spectrum

In the following, we present the measurement and data evaluation procedures for the characterization of the 2DEG-QD system and the investigation of its time response. Further details on the techniques can be found in Refs. 16 and 17.

We monitor the 2D channel conductance between the source and drain contacts, G_{SD}, using an 8 mV bias. The time-resolved response of the sample is recorded by applying rectangular pulses of $\Delta V_G = 20$ mV to the gate (Fig. 2, top). In addition, a constant charging bias V_G is applied to the gate that shifts the potential energy of the dots with respect to the back contact from which the electrons are tunneling. Thus, with increasing voltage, more and more electrons can be transferred from the back contact into the dots by tunneling through the barrier separating back contact and dots. As indicated in the insets to Fig. 2, bottom, when the Fermi energy of the 2DEG, E_F, is in resonance with an n-particle state E_n, single electrons can transfer into the dots during the "high" state of the pulse and out of the dots during the "low" state. The response time of the 2DEG is on the order of $t_{2D} \approx 1\,\mu$s, significantly faster than typical tunneling times $t_{QD} \approx 1 \rightarrow 3$ ms. Hence it is found that, when the probe voltage is applied, the conductance increases abruptly as the electron density in the 2DEG is increased by the field-effect. Then, on a slower time scale, electrons are tunneling into the dots, which lowers the electron density again and the conductance in the channel decreases exponentially until a steady value is reached (see Fig. 2, bottom). When the initial voltage is applied again, E_n is lifted above the Fermi level. The n-th electron is removed from the dot, the channel conductance increases accordingly. When the Fermi level E_F lies in the gap between two QD energy states, electron tunneling does not take place. In that case, the conductance exhibits an almost rectangular response, without the exponential transients from the tunneling dynamics. When increasing the charging bias from −0.9 to +0.4 V, up to six electrons can be loaded into each dot. The amplitude of the exponential decay during the high state, $\Delta G = G(t = 0) - G(t \rightarrow 0.06\,\mathrm{s})$ is evaluated and recorded as a function of the charging bias, as shown in Fig. 3.

From Fig. 3, we find that two lower energy peaks located at −0.67 and −0.53 V, and four peaks between −0.15 and 0.15 V.

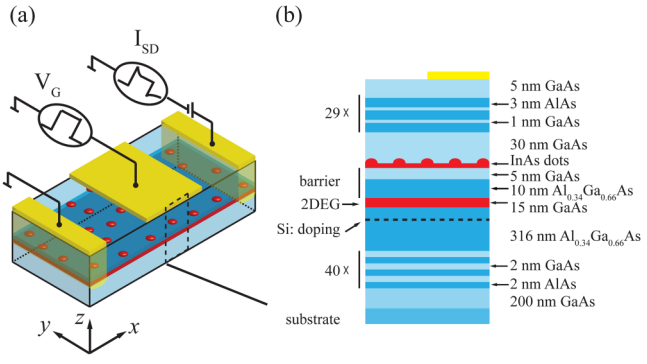

FIG. 1. (a) Fabricated transistor structure with source, drain, and gate electrode. A square pulse is applied on the gate to modify the quantum dot energy. The 2DEG conductance is recorded to monitor the charging of the quantum dots. (b) Schematic cross section of the layer sequence grown by molecular beam epitaxy.

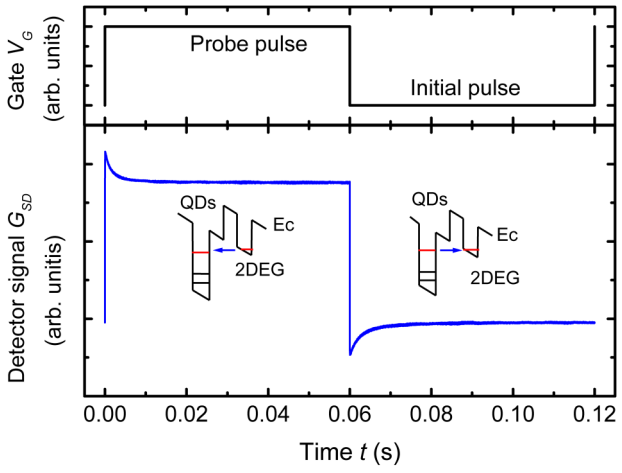

FIG. 2. Time-resolved conductance measurement. (top) A voltage pulse is applied to the gate. (bottom) The channel conductance is recorded every 8 μs. At the probe pulse, the carrier density in the back contact increases abruptly. The quantum dot state aligns with the Fermi level in the back contacts. When the n-th electron is transferred into the quantum dots, the source-drain conductance decreases exponentially. At the initial pulse, the conductance drops rapidly, which is followed by the increasing conductance as the n-th electron tunnels back from the QD into the 2DEG.

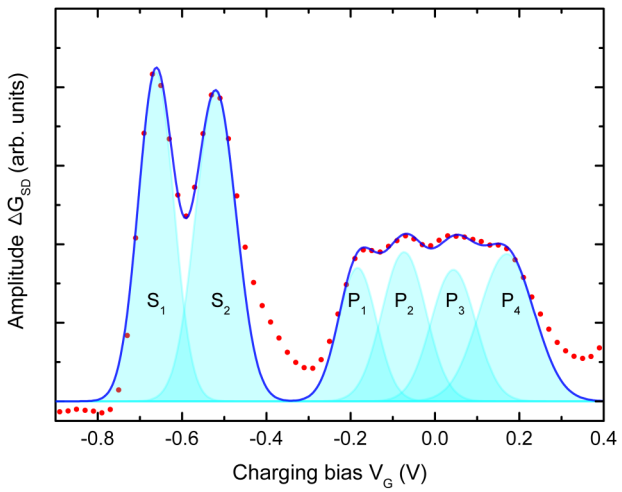

FIG. 3. Data points measured conductance change due to charge transfer into the QDs. Shaded areas are Gaussian fits on each state, and solid blue line is the summation of all fits.

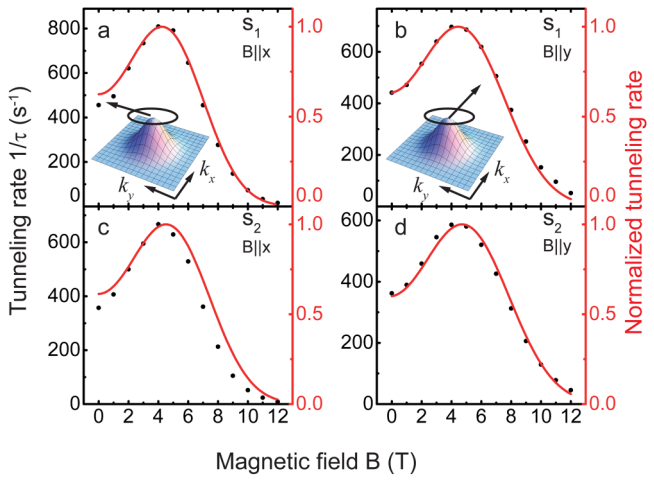

FIG. 4. Data points of measured tunneling rate as a function of magnetic field for two orthogonal field directions along $(1\bar{1}0)$ and (110) (left and right column, respectively). Lines are the calculated probabilities for dot dimensions (s_1: $l_x = 6.8$ nm, $l_y = 8$ nm, $k_F = 1.9 \times 10^8$ m^{-1}; s_2: $l_x = 6.7$ nm, $l_y = 7.5$ nm, $k_F = 2.0 \times 10^8$ m^{-1}). Insets indicate how the Fermi circle lines up with the dot wave function. Optimum momentum matching is achieved when the momentum shift approximately equals k_F.

Each peak corresponds to the charging of an additional electron into the QDs. The first two electrons form the so-called s-shell with two states, s_1 and s_2. The higher four peaks p_1 to p_4 constitute the p-shell.[9,19–21] We can convert the gate voltage into the energy by assuming that the energetic position of the dots changes linearly with respect to the Fermi energy pinned by the high charge density in the back contact. In other words, a change in gate voltage ΔV_G implies a change in energy as $\Delta E = e\Delta V_G/\lambda$, where λ, the lever arm is 7 for the present devices. This way, we can obtain the energy gap between s_1 and s_2 of 20 and 11 meV between the successive p-states. The gaps between the n-electron states within each shell are caused by Coulomb interaction while the larger gap between the shells also includes the quantization energy.[22]

B. The tunneling rate of s-like states

It is found that the change in conductivity $\Delta G(t) = G(t = 0) - G(t)$ can be well described by an exponential decay: $\Delta G(t) = G_0 e^{-t/\tau}$.[23] We will now evaluate the time constant τ, from which we can obtain the tunneling rate $(1/\tau)$ between the quantum dot and the 2DEG. In order to study the tunneling rate of individual states in detail, we can apply a magnetic field in plane of the quantum dot layer.

For the s_1 state, we use a probe pulse voltage of -0.67 V. The magnetic field is applied in the main crystal orientations $\mathbf{B} \parallel (110)$ or $\mathbf{B} \parallel (1\bar{1}0)$. The data points in Fig. 4 summarize the obtained tunneling rates $1/\tau$ as a function of B, applied along the two orthogonal directions [Figs. 4(a) and 4(b), where $\mathbf{x}$ and $\mathbf{y}$ correspond to the $(1\bar{1}0)$ and (110) crystal axes, respectively]. In agreement with previous studies,[23,24] we observe that the rate of tunneling into the lowest dot state increases with magnetic fields up to $B \approx 4.5$ T. With higher magnetic fields, the tunneling rate decreases monotonously. For the s_2 state, a similar result is obtained [as shown in Figs. 4(c) and 4(d)].

Similar studies on the subject of momentum match were performed by researchers from the University of Nottingham. For example, utilizing the double barrier resonant tunneling diode structure, they studied the momentum coupling principles extensively: between 2D quantum wells (2D → 2D),[25,26] between quantum wires (1D → 1D),[27] or between 3D emitters and quantum dots (3D → 0D),[28–32] respectively. Furthermore, they recognized the eigenenergies and wavefunctions of the quantum confined states. It is worth noting that, regarding the s state in the 3D → 0D system, the tunneling current maximum occurs in the absence of the magnetic field and degrades monotonously with a higher magnetic field, which are essentially different from our results. In samples with a 3D emitter, the tunneling current is mainly contributed from electrons with maximum k_z momentum (z is the tunneling direction), in other words, for $B = 0$, the tunneling electrons from the back contact have zero in-plane momentum $(k_x = k_y = 0)$.[13,28,29,33–35] However, in the case of a 2D emitter, the electrons at the Fermi energy in the back contacts have an in-plane momentum $k_\parallel = \sqrt{k_x^2 + k_y^2} = k_F = \sqrt{2\pi n_s}$, where the Fermi momentum k_F is given by the carrier density n_s in the 2D back contact. The s state wave function in the quantum dots has a Gaussian shape in momentum space, with maximum at $k_\parallel = 0$.[22,36] In a magnetic field, when an electron tunnels from the emitter into the dot, it acquires an additional in-plane momentum given by $\Delta k = eB_\parallel \Delta z/\hbar$, where Δz is the effective distance tunneling along $\mathbf{z}$ and $\hbar$ is the reduced Planck constant.[28,37] The momentum is acquired by the tunneling electron as a result of the Lorentz force. In terms of mapping out the shape of an electronic state, we can envisage the effect of the shift in k space as analogous to that of the displacement in real space of the atomic tip in an STM imaging measurement.[38,39]

The tunneling rate is proportional to the overlap of the wave functions in the QD and the 2DEG at the Fermi surface. To discuss the measurement data in depth, we follow the approach in Refs. 23 and 24 to calculate the overlap integral of the wave functions in the 2DEG and the quantum dot as $\left|\langle\psi_{2\mathrm{DEG}}|\psi_{\mathrm{QD}}\rangle\right|^2$. First, we consider the free electrons in the back contact. When **B** is parallel to the x axis, $\mathbf{B} = (B, 0, 0)$, using Landau gauge, the magnetic vector potential can be written as $\mathbf{A} = (0, -Bz, 0)$. Solving the Schrödinger equation, the electron eigenenergies are

$$E = E_z^* + \frac{\hbar^2}{2m}\left(k_x^2 + k_y^2\frac{E_z^2}{E_z^{*2}}\right), \tag{1}$$

where ω_c is the cyclotron frequency. $E_z^* = \hbar\sqrt{\omega_z^2 + \omega_c^2/4}$ is the diamagnetic shift, and $E_z = \hbar\omega_z$ is the bare confinement energy of the 2D quantum well, where we have assumed a parabolic confinement for simplicity. In our present case, the confinement energy is much stronger than the cyclotron energy, hence $E_z \approx E_z^*$. Equation (1) can be reduced to the usual dispersion of a 2D free electron gas. Similar to the quantum well, the wave functions of the quantum dots do not change noticeably in the magnetic field. We therefore only need to consider the Lorentz effect during the tunneling process.

The confinement potential of the dots can be described using a 2D simple harmonic oscillator, which has been proved to be an accurate model.[15,22] The s state wave function is

$$\psi_s = \sqrt{\frac{1}{l_x l_y \pi}}\cdot e^{-\frac{x^2}{2l_x^2}-\frac{y^2}{2l_y^2}}, \tag{2}$$

where l_x and l_y are the characteristic lengths of the confinement potential along the $(1\bar{1}0)$ and (110) directions. Following the discussion above, the emitter wave functions are taken to be plane waves with momentum k_F,

$$\psi_{2\mathrm{D}} = e^{ik_{x,\mathrm{F}}x + ik_{y,\mathrm{F}}y}, \tag{3}$$

where $k_{x,\mathrm{F}}$ and $k_{y,\mathrm{F}}$ are the x and y momentum components of the initial state at the emitter Fermi surface, $k_F^2 = k_{x,\mathrm{F}}^2 + k_{y,\mathrm{F}}^2$. The overlap integral is calculated numerically and summed up over the shifted Fermi circle introduced by the in-plane magnetic field.

The lines in Fig. 4 show the calculated results for the tunneling rates. In the evaluation, the quantum dot has been assumed to be elliptical. The confinement energy in the x direction is higher than that in the y direction, $l_x < l_y$. It can be seen, that all the experimental data points are reproduced well (with $\Delta z = 24$ nm; for s_1: $l_x = 6.8$ nm, $l_y = 8$ nm and $k_\mathrm{F} = 1.9 \times 10^8\ \mathrm{m}^{-1}$; for s_2: $l_x = 6.7$ nm, $l_y = 7.5$ nm and $k_\mathrm{F} = 2.0 \times 10^8\ \mathrm{m}^{-1}$). In the upper part of Fig. 4, the magnetic field is applied in the x direction. At zero magnetic fields, the Fermi circle aligns with the QD wave function. Because the radius of the Fermi circle is larger than the characteristic length of the dot wave function in momentum space (see the inset in Fig. 4), the tunneling rate is low. When increasing the magnetic field, the Fermi circle shifts along the y direction so that some part of the Fermi circle start to overlap with the maximum of the dot wave function. Therefore, the overall integral increases. At around $B = 5.2$ T, $\Delta k = k_\mathrm{F}$, the Fermi circle moves across the maximum of the QD wave function, the overlap value decreases again with increasing magnetic field.

C. The p state tunneling rate

While the s state wave functions in these quantum dots are of a simple, almost circular Gaussian shape, the p states are richer in features and reveal more specifics of the confining potential.[21] Figure 5(a) shows the tunneling rate of the p_1 state when the

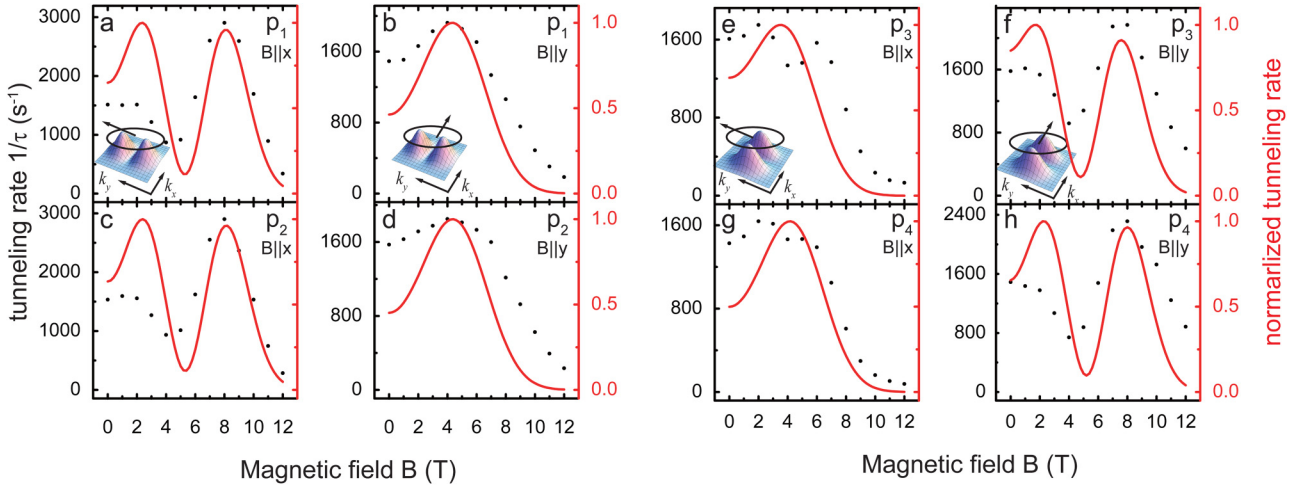

FIG. 5. Data points of measured tunneling rate as a function of magnetic field for two orthogonal field directions along $(1\bar{1}0)$ and (110). Lines are the calculated probabilities for the fixed tunneling distance $\Delta z = 24$ nm and the fitting parameters are: p_1: $l_x = 9.5$ nm, $l_y = 9.9$ nm, $k_\mathrm{F} = 2.05 \times 10^8\ \mathrm{m}^{-1}$; p_2: $l_x = 9.5$ nm, $l_y = 9.9$ nm, $k_\mathrm{F} = 2.06 \times 10^8\ \mathrm{m}^{-1}$; p_3: $l_x = 9.9$ nm, $l_y = 9.9$ nm, $k_\mathrm{F} = 1.85 \times 10^8\ \mathrm{m}^{-1}$; p_4: $l_x = 9.9$ nm, $l_y = 9.9$ nm, $k_\mathrm{F} = 2.0 \times 10^8\ \mathrm{m}^{-1}$.

magnetic field is along the x direction. As the magnetic field increases from 0 to 12 T, there is a minimum at around 4 T. The tunneling maximum occurs at 8 T. Figure 5(b) is the result when the magnetic field is along the y direction. Here, the magnetic field dependence is very similar to that of the s-states. Together, Figs. 5(a) and 5(b) show that the circular symmetry of the potential is sufficiently broken, so that the lowest p-state has a node in the y-direction, while the wave function looks similar to the ground state (≈Gaussian) along the x axis [see also the insets in Figs. 5(a) and 5(b)].

There are now two possibilities for the charging of the next electron: Either, the p_2 electron will go into the same orbital state as the p_1 electron, but with opposite spin, or Hund's rules will apply so that the spins align and the p_2 electron will occupy the orthogonal orbital state, with a node in the x-direction. Figures 5(c) and 5(d) clearly show that the node of the p_2 state is along the same axis as that of the p_1 state. Therefore, we find that Hund's rules do not apply for the present, slightly asymmetric quantum dots, in agreement with previous results.[21]

Extending the discussion of the p_1 and p_2 electrons, we expect the next two electrons (p_3, p_4) to also occupy the same orbital state, which is, however, orthogonal to the orbital of the lower p-electrons [see insets in Figs. 5(e) and 5(f)]. Indeed, the experimental results in Figs. 5(e)–5(h) support this prediction: The magnetic-field dependence of the tunneling rate into p_3 and p_4 resembles that for p_1 and p_2, but with interchanged x and y axes.

Next, we will explain the curve shape in the magnetic fields. As before, we use the harmonic oscillator as an approximation for the confining potential. Then, the p state wave functions can be approximated as

$$\psi_{p_-} = \sqrt{\frac{2}{l_x l_y \pi}} \cdot \frac{y}{l_y} \cdot e^{-\frac{x^2}{2l_x^2} - \frac{y^2}{2l_y^2}}, \tag{4a}$$

$$\psi_{p_+} = \sqrt{\frac{2}{l_x l_y \pi}} \cdot \frac{x}{l_x} \cdot e^{-\frac{x^2}{2l_x^2} - \frac{y^2}{2l_y^2}}. \tag{4b}$$

Here, p_- is the orbital wave function with a lower energy, with a node in the y-direction (p_1 and p_2 electron). The p_+ orbital accounts for the two higher energy electrons, p_3 and p_4.

The calculation results are presented as solid lines in Fig. 5. The agreement between the calculation and measured data is not as good as for the s state, but the model reproduces the varying trends well. This can be attributed to two reasons regarding the real system: (1) the wave functions that are occupied by electrons in the measurement are selected via the gate voltage pulse. This has a pulse height of $\Delta V_G = 20$ mV. With the already mentioned lever arm of 7, this results in an energy change of about 3 meV. All wave functions that lie within this energy range contribute to the detected tunneling processes. (2) The quantum dots in the ensemble have a typical non-uniformity. This leads to an inhomogeneous broadening of the states in the charging spectrum. In Fig. 3, it can be seen that for the p states, the width roughly corresponds to the splitting of the states themselves (voltage difference $\Delta V_G \approx 100$ mV corresponds to $\Delta E \approx 15$ meV). This overlap of the states leads to the fact that in the measurements also the wave function with the opposite orientation is sampled. This can be seen, for example, for the tunneling rates at about 4 T in Figs. 5(a), 5(c), 5(e), and 5(g). For states p_1 and p_2, a minimum is present, but it is weaker than that would be expected for the p_- wave function. At the same time, the states p_3 and p_4 show a small local minimum in this direction, although a clear global maximum is to be expected there for the p_+ wave function.

D. Comparison of the charging and emission rates

In the former sections, we have discussed the tunneling rate based on the charging process, corresponding to the exponential decrease between $t = 0$ and $t = 0.06$ s in Fig. 2. In the following, we will compare these data with the emission rates, evaluated from the data, when the dots are discharged again ($0.06\,\text{s} < t < 0.12\,\text{s}$). The charging and emission rates at zero magnetic field under different gate voltages are presented in Fig. 6. From the figure, we can distinguish the s and p shells clearly. The tunneling times between the 2DEG and the dots are in the order $\tau_s = 3$ ms and $\tau_p = 0.8$ ms for the s and p states, respectively. Comparing the tunneling rate for discrete states, we can find that, the charging rate of s_1 is higher than the emission rate. However, for the s_2 state, the charging rate is slower than the emission rate. Furthermore, it is found that the charging rates of p_1 and p_3 are higher than the emission rates, and that the charging rates of p_2 and p_4 are lower than emission rates. In other words, when the electron number n in the quantum dot is odd, the charging rate is faster, otherwise, the emission rate is faster. This even–odd sequence strongly suggests that the behavior can be attributed to spin effects. Because we have x–y symmetry and Hund's rules do not apply, the six electrons are distributed onto three orbital states, s, p_-, and p_+, which each can be occupied with

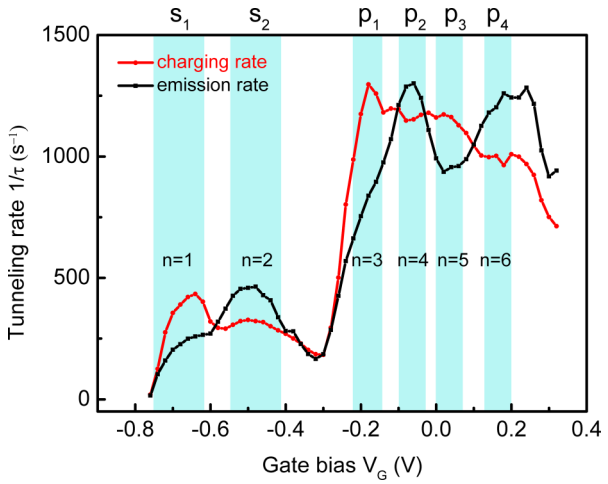

FIG. 6. Tunneling rates vs gate bias without magnetic field. The rate for the p states is about three times faster than for the s-state. The charging rate is faster than the emission rate when the electron number n in the dot is even, but the charging rate is lower than the emission rate when n is odd.

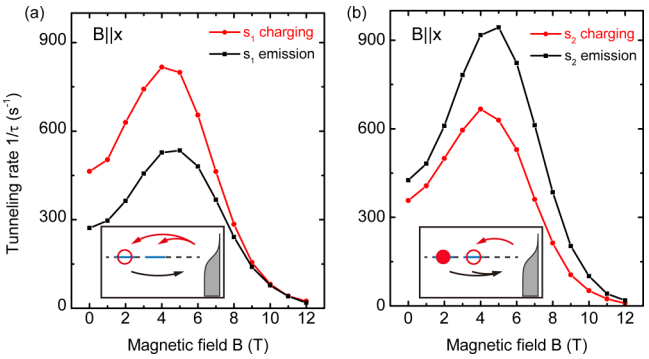

FIG. 7. Comparison of the charging and emission rates of the first two electrons as a function of magnetic field. The insets show the adding and removing electron process in the *s* shell of twofold degeneracy.

one or two electrons. When the first electron is charging an orbital state (odd n), it has two possible spin states to tunnel into. Discharging, on the other hand, can only take place out of the singly occupied state. For even n, the situation is reversed: Only one state is available for tunneling into the dot, while discharging can take place out of two states. So, we can find that the emission rate of the second electron in each group is faster than the charging rate.[21]

Finally, in Fig. 7, we present the s_1 and s_2 tunneling rates in the magnetic fields. From the results, we see that the above discussion about the different rates also holds for tunneling in parallel magnetic fields. Under all magnetic fields, the s_1 charging rate is faster than the emission rate [see Fig. 7(a)], and the case is inverted for s_2 charging rate [see Fig. 7(b)]. In addition, for either of the two states, the difference between charging and emission rates is prominent under the low magnetic fields, but it becomes weaker when $B > 8$ T. The schematic tunneling processes for the charging and emission are given in the insets. For the first electron, the QD is initially empty, so there are two possible states to tunnel into the QD, but only one way to remove an electron once one electron has tunneled into the QD. For the second electron, the shell is already occupied with one electron, so there is only one way to tunnel into the dot, but either electron may be removed.

III. CONCLUSION

In summary, we have studied the tunneling rate between quantum dots and a 2DEG. The tunneling rate strongly depends on the momentum matching of the two systems. For either the *s* or the *p* state, the application of a magnetic field perpendicular to the tunnel path can be used to offset the momentum mismatch and increase the tunneling rate. In higher magnetic fields, the tunneling rate can be strongly suppressed due to the mismatch. An asymmetric confinement of quantum dots is found in the wave function of the *s* state from the shift of the Fermi circle in the magnetic field. The result agrees well with the node distribution of *p* state wave functions. Furthermore, it is also observed that the spin degeneracy leads to an odd–even oscillation in the ratio of the charging and emission rates.

ACKNOWLEDGMENTS

This work was funded by the Deutsche Forschungsgemeinschaft (DFG, German Research Foundation) Project-ID 278162697 SFB 1242 and the individual research Grant Nos. GE2141/5-1 and LU2051/1-1. Ar. L. and A.D.W. acknowledge gratefully support of DFG-TRR-160, BMBF-Q.Link.X 16KIS0867, and the DFH/UFA CDFA-05-06. D. Zhou would like to acknowledge the China Scholarship Council (CSC) for financial support.

AUTHOR DECLARATIONS

Conflict of Interest

The authors have no conflicts to disclose.

Author Contributions

Daming Zhou: Data curation (lead); Formal analysis (lead); Funding acquisition (equal); Writing – original draft (lead). **Jens Kerski:** Formal analysis (equal); Writing – original draft (equal); Writing – review and editing (equal). **Andreas Beckel:** Data curation (equal); Formal analysis (equal); Writing – original draft (equal); Writing – review and editing (equal). **Martin Geller:** Formal analysis (equal); Writing – review and editing (supporting). **Axel Lorke:** Funding acquisition (equal); Supervision (lead); Writing – original draft (equal); Writing – review and editing (equal). **Arne Ludwig:** Funding acquisition (equal); Resources (equal); Writing – review and editing (supporting). **Andreas D. Wieck:** Funding acquisition (equal); Resources (equal); Writing – review and editing (supporting). **Xiaoshuang Chen:** Supervision (equal); Writing – review and editing (supporting). **Wei Lu:** Supervision (equal); Writing – review and editing (supporting).

DATA AVAILABILITY

The data that support the findings of this study are available from the corresponding author upon reasonable request.

REFERENCES

[1]K. Koike, K. Saitoh, S. Li, S. Sasa, M. Inoue, and M. Yano, "Room-temperature operation of a memory-effect AlGaAs/GaAs heterojunction field-effect transistor with self-assembled InAs nanodots," Appl. Phys. Lett. **76**, 1464 (2000).
[2]C. Balocco, A. M. Song, and M. Missous, "Room-temperature operations of memory devices based on self-assembled InAs quantum dot structures," Appl. Phys. Lett. **85**, 5911 (2004).
[3]D. Nataraj, N. Ooike, J. Motohisa, and T. Fukui, "Fabrication of one-dimensional GaAs channel-coupled InAs quantum dot memory device by selective-area metal-organic vapor phase epitaxy," Appl. Phys. Lett. **87**, 193103 (2005).
[4]C. R. Müller, L. Worschech, J. Heinrich, S. Höfling, and A. Forchel, "Room temperature memory operation of a single InAs quantum dot layer in a GaAs/AlGaAs heterostructure," Appl. Phys. Lett. **93**, 063502 (2008).
[5]A. Marent, T. Nowozin, M. Geller, and D. Bimberg, "The QD-Flash: A quantum dot-based memory device," Semicond. Sci. Tech. **26**, 014026 (2010).
[6]T. Nowozin, A. Beckel, D. Bimberg, A. Lorke, and M. Geller, "3 ns single-shot read-out in a quantum dot-based memory structure," Appl. Phys. Lett. **104**, 053111 (2014).
[7]S. T. Yılmaz, P. Fallahi, and A. Imamoğlu, "Quantum-dot-spin single-photon interface," Phys. Rev. Lett. **105**, 033601 (2010).

[8]T. Gao, L. Rickert, F. Urban, J. Große, N. Srocka, S. Rodt, A. Musiał, K. Żołnacz, P. Mergo, K. Dybka, W. Urbańczyk, G. Sęk, S. Burger, S. Reitzenstein, and T. Heindel, "A quantum key distribution testbed using a plug&play telecom-wavelength single-photon source," Appl. Phys. Rev. **9**, 011412 (2022).
[9]H. Drexler, D. Leonard, W. Hansen, J. P. Kotthaus, and P. M. Petroff, "Spectroscopy of quantum levels in charge-tunable InGaAs quantum dots," Phys. Rev. Lett. **73**, 2252 (1994).
[10]M. Fricke, A. Lorke, J. P. Kotthaus, G. Medeiros-Ribeiro, and P. M. Petroff, "Shell structure and electron-electron interaction in self-assembled InAs quantum dots," Europhys. Lett. **36**, 197 (1996).
[11]B. T. Miller, W. Hansen, S. Manus, R. J. Luyken, A. Lorke, J. P. Kotthaus, S. Huant, G. Medeiros-Ribeiro, and P. M. Petroff, "Few-electron ground states of charge-tunable self-assembled quantum dots," Phys. Rev. B **56**, 6764 (1997).
[12]R. J. Luyken, A. Lorke, A. O. Govorov, J. P. Kotthaus, G. Medeiros-Ribeiro, and P. M. Petroff, "The dynamics of tunneling into self-assembled InAs dots," Appl. Phys. Lett. **74**, 2486 (1999).
[13]W. Lei, C. Notthoff, J. Peng, D. Reuter, A. Wieck, G. Bester, and A. Lorke, "'Artificial atoms' in magnetic fields: Wave-function shaping and phase-sensitive tunneling," Phys. Rev. Lett. **105**, 176804 (2010).
[14]B. Marquardt, M. Geller, A. Lorke, D. Reuter, and A. D. Wieck, "Using a two-dimensional electron gas to study nonequilibrium tunneling dynamics and charge storage in self-assembled quantum dots," Appl. Phys. Lett. **95**, 022113 (2009).
[15]B. Marquardt, M. Geller, B. Baxevanis, D. Pfannkuche, A. D. Wieck, D. Reuter, and A. Lorke, "Transport spectroscopy of non-equilibrium many-particle spin states in self-assembled quantum dots," Nat. Commun. **2**, 209 (2011).
[16]A. Beckel, A. Ludwig, A. D. Wieck, A. Lorke, and M. Geller, "Time-resolved transconductance spectroscopy on self-assembled quantum dots: Spectral evolution from single-into many-particle states," Phys. Rev. B **89**, 155430 (2014).
[17]K. Eltrudis, A. Al-Ashouri, A. Beckel, A. Ludwig, A. D. Wieck, M. Geller, and A. Lorke, "All-electrical measurement of the triplet-singlet spin relaxation time in self-assembled quantum dots," Appl. Phys. Lett. **111**, 092103 (2017).
[18]M. Geller, "Nonequilibrium carrier dynamics in self-assembled quantum dots," Appl. Phys. Rev. **6**, 031306 (2019).
[19]P. M. Petroff, A. Lorke, and A. Imamoglu, "Epitaxially self-assembled quantum dots," Phys. Today **54**, 46 (2001).
[20]L. Cockins, Y. Miyahara, S. D. Bennett, A. A. Clerk, S. Studenikin, P. Poole, A. Sachrajda, and P. Grutter, "Energy levels of few-electron quantum dots imaged and characterized by atomic force microscopy," Proc. Natl. Acad. Sci. U.S.A. **107**, 9496 (2010).
[21]A. Beckel, A. Kurzmann, M. Geller, A. Ludwig, A. D. Wieck, J. König, and A. Lorke, "Asymmetry of charge relaxation times in quantum dots: The influence of degeneracy," Europhys. Lett. **106**, 47002 (2014).
[22]R. J. Warburton, B. T. Miller, C. S. Dürr, C. Bödefeld, K. Karrai, J. P. Kotthaus, G. Medeiros-Ribeiro, P. M. Petroff, and S. Huant, "Coulomb interactions in small charge-tunable quantum dots: A simple model," Phys. Rev. B **58**, 16221 (1998).
[23]A. Beckel, D. Zhou, B. Marquardt, D. Reuter, A. D. Wieck, M. Geller, and A. Lorke, "Momentum matching in the tunneling between 2-dimensional and 0-dimensional electron systems," Appl. Phys. Lett. **100**, 232110 (2012).
[24]D. Zhou, A. Beckel, A. Ludwig, A. D. Wieck, M. Geller, and A. Lorke, "Tuning the tunneling probability between low-dimensional electron systems by momentum matching," Appl. Phys. Lett. **106**, 243105 (2015).
[25]J. Wang, P. H. Beton, N. Mori, L. Eaves, H. Buhmann, L. Mansouri, P. C. Main, T. J. Foster, and M. Henini, "Resonant magnetotunneling via one-dimensional quantum confined states," Phys. Rev. Lett. **73**, 1146 (1994).
[26]N. Mori, P. H. Beton, J. Wang, and L. Eaves, "Theory of resonant tunneling through a quantum wire," Phys. Rev. B **51**, 1735 (1995).
[27]P. H. Beton, J. Wang, N. Mori, L. Eaves, P. C. Main, T. J. Foster, and M. Henini, "Measuring the probability density of quantum confined states," Phys. Rev. Lett. **75**, 1996 (1995).
[28]E. E. Vdovin, A. Levin, A. Patanè, L. Eaves, P. C. Main, Y. N. Khanin, Y. V. Dubrovskii, M. Henini, and G. Hill, "Imaging the electron wave function in self-assembled quantum dots," Science **290**, 122 (2000).
[29]A. Patanè, R. J. A. Hill, L. Eaves, P. C. Main, M. Henini, M. L. Zambrano, A. Levin, N. Mori, C. Hamaguchi, Y. V. Dubrovskii, E. E. Vdovin, D. G. Austing, S. Tarucha, and G. Hill, "Probing the quantum states of self-assembled InAs dots by magnetotunneling spectroscopy," Phys. Rev. B **65**, 165308 (2002).
[30]G. Allison, N. Mori, A. Patanè, J. E. L. Eaves, D. K. Maude, and M. Hopkinson, "Strong effect of resonant impurities on Landau-level quantization," Phys. Rev. Lett. **96**, 236802 (2006).
[31]O. Makarovsky, O. Thomas, A. G. Balanov, L. Eaves, A. Patanè, R. P. Campion, C. T. Foxon, E. E. Vdovin, D. K. Maude, G. Kiesslich, and R. J. Airey, "Fock-Darwin-like quantum dot states formed by charged Mn interstitial ions," Phys. Rev. Lett. **101**, 226807 (2008).
[32]N. Mori, A. Patanè, and L. Eaves, "Theory of resonant tunneling through a donor state," Jpn. J. Appl. Phys. **51**, 02BJ02 (2012).
[33]M. Rontani and E. Molinari, "Imaging quasiparticle wave functions in quantum dots via tunneling spectroscopy," Phys. Rev. B **71**, 233106 (2005).
[34]O. S. Wibbelhoff, A. Lorke, D. Reuter, and A. D. Wieck, "Magnetocapacitance probing of the many-particle states in InAs dots," Appl. Phys. Lett. **86**, 092104 (2005).
[35]G. Bester, D. Reuter, L. He, A. Zunger, P. Kailuweit, A. D. Wieck, U. Zeitler, J. C. Maan, O. Wibbelhoff, and A. Lorke, "Experimental imaging and atomistic modeling of electron and hole quasiparticle wave functions in InAs/GaAs quantum dots," Phys. Rev. B **76**, 075338 (2007).
[36]M. A. Cusack, P. R. Briddon, and M. Jaros, "Electronic structure of InAs/GaAs self-assembled quantum dots," Phys. Rev. B **54**, R2300 (1996).
[37]J. Smoliner, W. Demmerle, G. Berthold, E. Gornik, G. Weimann, and W. Schlapp, "Momentum conservation in tunneling processes between barrier-separated 2D-electron-gas systems," Phys. Rev. Lett. **63**, 2116 (1989).
[38]B. Grandidier, Y. M. Niquet, B. Legrand, J. P. Nys, C. Priester, D. Stiévenard, J. M. Gérard, and V. Thierry-Mieg, "Imaging the wave-function amplitudes in cleaved semiconductor quantum boxes," Phys. Rev. Lett. **85**, 1068 (2000).
[39]T. Maltezopoulos, A. Bolz, C. Meyer, C. Heyn, W. Hansen, M. Morgenstern, and R. Wiesendanger, "Wave-function mapping of InAs quantum dots by scanning tunneling spectroscopy," Phys. Rev. Lett. **91**, 196804 (2003).